Delicate control of crystallographic facet-oriented Cu_2O nanocrystals and the correlated adsorption ability†

Dong-Feng Zhang,[a] Hua Zhang,[a] Lin Guo,*[a] Kun Zheng,[b] Xiao-Dong Han*[b] and Ze Zhang[b]

Received 18th September 2008, Accepted 8th May 2009
First published as an Advance Article on the web 12th June 2009
DOI: 10.1039/b816349a

In this work, we demonstrate the systematic and delicate geometry control of Cu_2O nanocrystals by taking advantage of the selective surface stabilization effect. A variety of Cu_2O architectures, evolved from cubes through truncated cubes, cubooctahedrons, truncated octahedrons and finally to octahedrons, were achieved by simply adjusting the added PVP. Based on the understanding of the intrinsic structural features of the cuprite Cu_2O and PVP, we elucidated the underlying shape evolution mechanism. The as-prepared products demonstrated a crystallography-dependent adsorption ability with methyl orange (MeO) as the pollutant. With the advantage of a low cost, high yield and straightforward procedure without pre-formed crystals as sacrificial templates, this method may provide a good starting point for the study of shape construction and morphology-dependent properties of other nanocrystals.

Introduction

To design and delicately control the shape of nanocrystals is one of the most important issues in nanoscience, chemistry and physics owing to the close correlations of the surface morphologies with the electronic structure, bonding, surface energy, and chemical reactivity.[1–5] The facets with different crystallographic characters have distinctive surface atomic structures, reconstructions, and atomic termination features corresponding to sharp differences that have been demonstrated in light-sensing, gas and chemical reactivity, field emission properties *etc*.[6–9] The ability to understand, predict and control the exposed surfaces and the corresponding volume fractions of nanocrystals is of critical importance to elucidate and explore shape-dependent chemical and physical properties.

The shape of a nanocrystal is determined by the opened facets and edges. It is generally accepted that the equilibrium form of a crystal tends to possess a minimal total surface energy.[10] The facets with the lowest surface energy will dominate the surfaces of a crystal. In principle, tuning the shape could be achieved by altering the relative order of the surface energy of different crystallographic facets. Preferential adsorption of organic or inorganic additives on certain crystallographic surfaces offers a good opportunity to tune and control the surface activities of nanomaterials. In recent years, great efforts were devoted to the controlled synthesis in the presence of various additives.[11–21] Cu_2O is an ideal compound to study the influence of electron correlation effects on the electronic structure particularly in high T_c superconductors. The rare occurrence of O–Cu–O 180-degree linear co-ordination of Cu_2O made its crystalline surfaces of {111}, {100} and {110} possess very distinctive chemical activities. Controlled fabrication of Cu_2O nanocrystallites has been one of the key issues in recent years.[12,17,18,22,23] Using cetyltrimethylammonium (CTAB) as the surfactant, Gou and Murphy fabricated regular oxide Cu_2O nanocubes.[12] Siegfried and Choi reported the shape transformation of the pre-grown Cu_2O cubes using sodium dodecyl sulfate (SDS) and inorganic ions as additives *via* an electrodeposition method.[22,23] However, how to precisely direct and control the surface facets by a simple and mild way remains a big challenge. This is not only important for achieving the accurate crystallographic facets with desired volume fractions but also necessary for understanding the effects of additives on the crystal growth behaviour of other oxides.

In this work, we successfully achieved the crystallographic surface control of Cu_2O nanocrystals by taking advantage of the selective surface stabilization of polyvinylpyrrolidone (PVP) on {111} surfaces of cuprite Cu_2O. The surface area ratio of {111} to {100} was delicately tuned by simply adjusting the amount of added PVP, which resulted in a systematic shape evolution and a variety of Cu_2O architectures were produced. The detailed modification mechanism was elucidated from the structural and dynamic point of view. The as-prepared Cu_2O polyhedrons exhibited a facet-related adsorption ability to MeO.

Experimental

All of the chemical reagents used in this experiment were of analytical grade and used without further purification. In a typical synthesis, given amounts of polyvinylpyrrolidone (PVP, M_W 30 000) were dissolved into an aqueous solution of $CuCl_2 \cdot 2H_2O$ (0.0l mol L^{-1}, 100 mL) for the desired R (R is defined as the molar ratio of PVP to $CuCl_2 \cdot 2H_2O$). Then, 10.0 mL NaOH aqueous solution (2.0 mol L^{-1}) was added dropwise into the above transparent light green solution. During the process, the solution color turned into turbid blue-green, and then dark brown. After stirring

[a]*School of Chemistry & Environment, Beijing University of Aeronautics and Astronautics, Beijing, 100083, China. E-mail: guolin@buaa.edu.cn; xdhan@bjut.edu.cn; Fax: +86-10-82338162; Tel: +86-10-82338162*
[b]*Institute of Microstructure and Properties of Advanced Materials, Beijing University of Technology, Beijing, 100022, China*

† Electronic supplementary information (ESI) available: The broad views and XRD patterns of different shaped Cu_2O polyhedrons, the detailed structure analysis and the FESEM images of different sized Cu_2O nanocubes and octahedraons. See DOI: 10.1039/b816349a

for 0.5 h, an ascorbic acid solution (10.0 mL, 0.6 M) was added dropwise into the dark brown solution. A turbid red liquid gradually formed. The mixture was aged for 3 h. All of the procedure was carried out under constant stirring and heated in a water bath at a given temperature. The resulting precipitate was collected by centrifugation and decanting, followed by washing with distilled water 3 times and absolute ethanol twice to remove the residual inorganic ions and polymer, and finally dried in vacuum at 60 °C for 5 h for further characterization. Concerning the investigation of the molecular weight effect, the other conditions were kept identical except for the molecular weight of the PVP that was used, *i.e.* 3.333 g PVPs with varying molecular weights (M_w 30 000, 58 000, and 630 000) were used as modifying agents. The detailed experimental conditions are listed in Table S1 (ESI†).

X-Ray powder diffraction (XRD, Rigaku, Dmax2200, Cu Kα) was used for the structural determination. Further microstructural analyses were performed using field-emission scanning electron microscopy (FESEM, Hitachi-S4300 with an accelerating voltage of 20 kV) and transmission electron microscopy (TEM, JEOL JEM-2100F with an accelerating voltage of 200 kV). UV-Vis spectra were recorded on a GBC Cintra-10e spectrophotometer.

The adsorption activities of the different shaped Cu_2O were investigated using methyl orange ($C_{14}H_{14}N_3NaO_3S$, MeO) as pollutant. Briefly, 0.05 g Cu_2O polyhedrons with different shapes were dispersed into an aqueous solution of MeO (100 mL, 15 mg L^{-1}). Under constant stirring in the dark, about 5 mL of the mixture solution was taken out at different intervals. After centrifugation, the UV-Vis spectrum of the supernatant was recorded to monitor the adsorption behavior. Fourier transform infrared spectroscopy (FT-IR, Nicolet, AVATAR360) was employed to characterize the residual MeO on the Cu_2O nanocrystals after adsorption.

Results and discussion

Scanning electron microscopy (SEM) observations (Fig. 1) clearly demonstrated the delicate geometry control that was achieved by simply adjusting the amount of added PVP. The broad views of the different shaped Cu_2O are shown in Fig. S1 (ESI†). In the absence of PVP, cube-shaped particles, the thermodynamically stable form of the cuprite Cu_2O, with diameters of about 900 nm, dominated the products (Fig. 1a). As shown by the three-dimensional (3-D) model (Fig. 1g), the exposed surfaces of the cubes are made of six {100} facets. When the molar ratio of PVP to $CuCl_2 \cdot 2H_2O$ (defined as *R*) was increased to 5, {111}-corner-truncated cubes (Fig. 1b) with an edge length of about 650 nm were produced, which is equal to a triangle with length of about 180 nm cut in each vertice of the cubes. With the *R* further increasing, the products experienced a shape evolution from cubooctahedrons (Fig. 1c) to vertex-truncated octahedrons (Fig. 1d and 1e) and finally to high symmetry octahedrons (Fig. 1f), corresponding to a progressive shrinkage of {100} and enlargement of {111} as illustrated by Fig. 1g–1i. The decreasing surface ratio of {100} to {111} (defined as *r*) was further confirmed by X-ray powder diffraction (XRD) characterization. All the diffraction peaks can be indexed to cuprite Cu_2O (JCPDS No. 77-0199) in spite of the deviation of the relative diffraction intensity (Fig. S2, ESI†). As shown in the inset of Fig. S2 (ESI†), the diffraction intensity ratio of (111)/(200) exhibited an obvious increase with the shape evolution from the cubes through truncated cubes, cubooctahedrons, truncated octahedrons and finally to octahedrons. SEM observation revealed that *R* is a key factor directing the morphology evolution of the Cu_2O nanocrystals.

The quantified crystallographic features regarding the exposed surfaces of these architectures were proved by TEM observations and the corresponding selected area electron diffraction (SAED) analysis viewed along a series of important low miller index directions. Fig. 2 presents the cubooctahedron as an example. As illustrated by the 3-D model (Fig. 2a), the cubooctahedron is bounded by six square {100} and eight triangle {111} facets. If the electron beam is aligned to be perpendicular to {001}, a two-dimensional square-shaped projection is observed (Fig. 2b). The truncation along [111] makes the corner parts thinner than the center part, which accounts for the bright contrast in the four

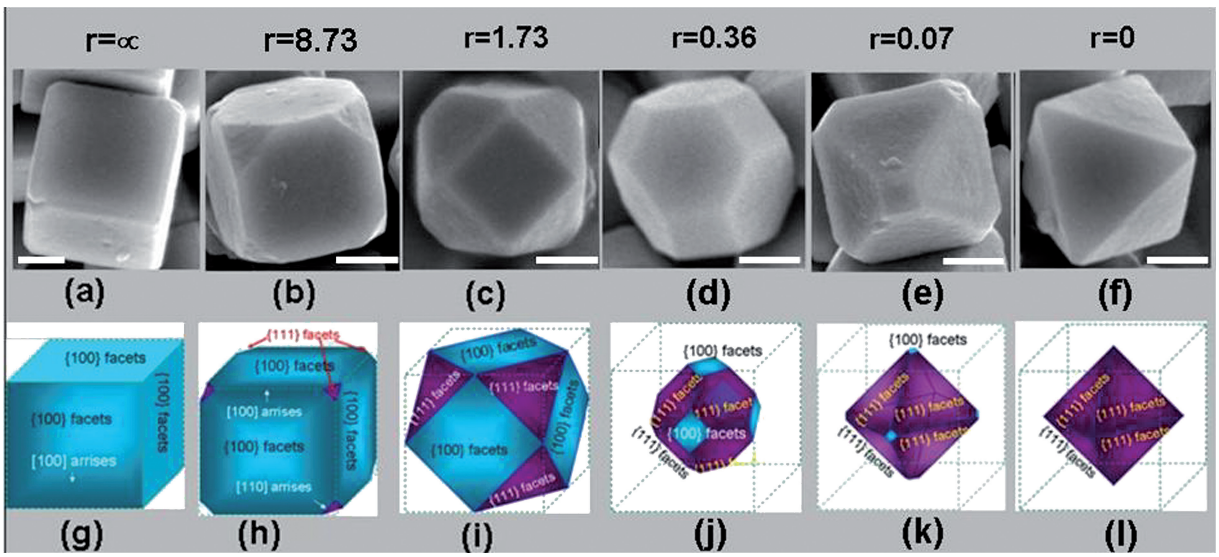

Fig. 1 FESEM images of the Cu_2O polyhedrons with different volume ratios of {100} to {111} (*r*). (a) $r = \infty$, (b) $r = 8.73$, (c) $r = 1.73$, (d) $r = 0.36$, (e) $r = 0.07$, (f) $r = 0$, (e–l) are the corresponding 3-D geometry models. Scale bar = 300 nm.

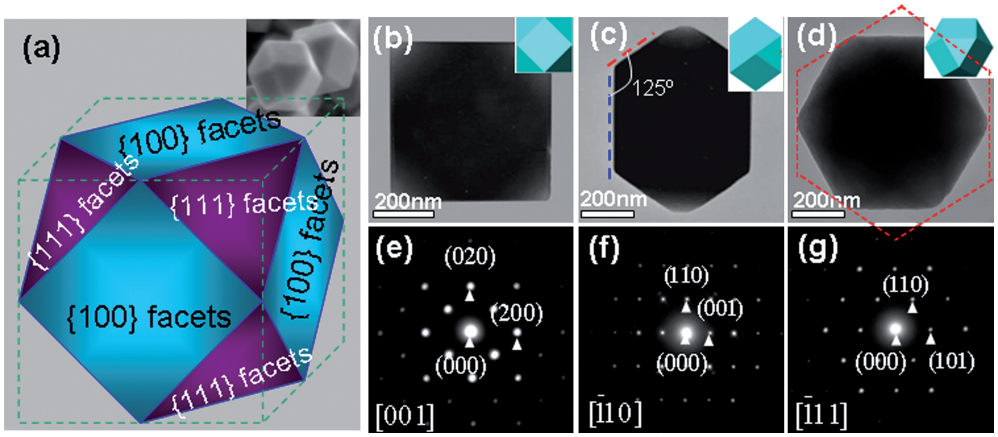

Fig. 2 The detailed crystallographic features of the Cu_2O cubooctahedrons. (a) The sketch, (b–d) the bright TEM images, and (e–g) the corresponding SAED patterns with the electron beams parallel to [001], [110], and [111], respectively.

vertex angles of the square. With [110] as the viewing direction, the projection changes into a hexagon (Fig. 2c), which is made of two {100} facets (blue dashed), and four {111} projections (red dashed). As indicated in Fig. 2c, the angle between the red dashed line and the blue dashed line is 125°, matching well with the crystallographic angle between (111) and (100) facets of the cubic Cu_2O. However, with <111> as the zone axis, the projection exhibits as an equilateral hexagon constructed by the edges of [100] and [110] (Fig. 2d). The corresponding diffraction patterns shown in Fig. 2e–2g provide solid evidence for the above descriptions. The detailed structural schemes of the cubic and octahedral particles are depicted in the supporting information (Fig. S3, ESI†).

In conjunction with the SEM observations (Fig. 1), it can be concluded that PVP had acted as a capping agent and that preferential adsorption occurred on the {111} planes of the Cu_2O crystals. By adjusting the adsorption kinetic of the surface activities on {111}, the volume ratio of {111} over {100} was delicately controlled, which resulted in the evolution process of the Cu_2O nanoarchitectures. We could gain some insight from the structural features and the crystal growth habit of the cuprite Cu_2O. Regarding the crystal growth, it is believed that the reduction of surface energy is the primary impetus for the morphology evolution.[24–26] The crystal growth rate perpendicular to a plane is proportional to its surface energy. For cuprite structured Cu_2O, each 'O' is surrounded by a tetrahedron of 'Cu', and each 'Cu' has two 'O' neighbors as illustrated by its unit cell model (Fig. 3a). The atomic arrangements along different crystallographic planes of Cu_2O are displayed in Fig. 3b to 3d. Structurally, the cuprite Cu_2O crystal can be described as layers of atoms stacking alternately and periodically. Along the [100] direction, the periodicity can be defined as two layers (layer 1 and layer 2 as shown in Fig. 3b). Layer 1 is composed of 'O' while 'Cu' atoms dominated layer 2. The alternating layers along the [110] direction can be described as entirely 'Cu' (layer 2 in Fig. 3c) or a mixture of 'O' and 'Cu' atoms arranged in a '–O–Cu–O–Cu-' sequence (layer 1 in Fig. 3c). In principle, layer 1 and layer 2 have equal possibility as a termination layer in both of these two cases. However, since the growth took place in aqueous media, 'Cu'-terminated would be rather unstable due to the active interaction

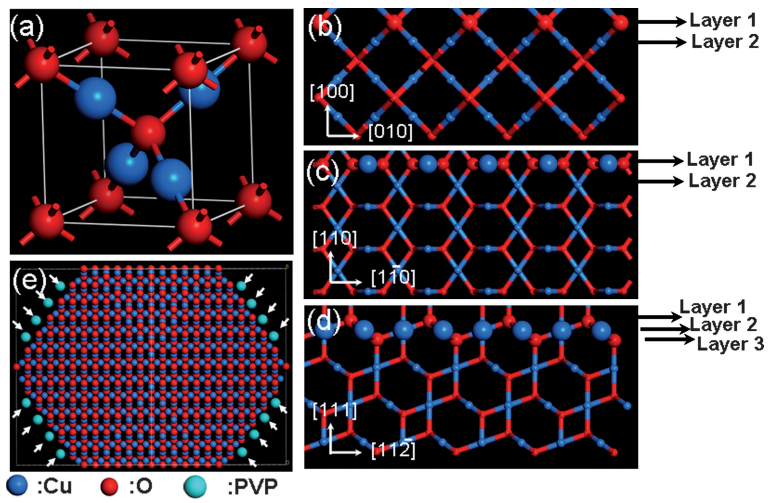

Fig. 3 (a) The unit cell of the cuprite Cu_2O, (b–d) the atomic arrangement in (100), (110), and (111) planes of the Cu_2O structure, respectively, and (e) the scheme showing the interaction of PVP with the (111) planes of the Cu_2O.

with the hydroxyl group. Thus, 'O'- and '–O–Cu–O–Cu–'-terminated surfaces are expected for {100} and {110} planes, respectively. With respect to the [111] direction, three atom layers consist of one period, where the 'Cu' layer is sandwiched between two layers of 'O' atoms. However, the distance between two adjacent layers in such a period is as short as $\frac{\sqrt{3}}{4}a$. So, the three layers can be approximately regarded as in the same surface. Every two 'Cu' atoms has a dangling bond perpendicular to the {111} planes. Regarding the crystallographic surface structure of Cu_2O, only {100} sets have 100% oxygen terminated surfaces and thus deduce a minimum energy state. This was evidenced by the cubic shape of Cu_2O crystals in the absence of PVP (Fig. 1a). Furthermore, we predict that {111} surfaces possess a high energy status due to the exposure of 'Cu' atoms with dangling bonds. To minimize the total surface energy, the introduced PVP would prefer to adsorb onto the higher energy surfaces {111}.

Although the added modifier, PVP, is a non-ionic surfactant, an easily polarized functional group '–C=O' is presented in its repeated unit. 'O', with a negative charge preferred to interact with positively charged 'Cu' to compensate the local surface charge imbalance and thus stabilize the crystal surfaces (Fig. 3e). Comparing with the 'O'-terminated {001} planes and the 'Cu'-coordination saturated {110} planes, the coordination unsaturated 'Cu' in the {111} surface is obviously more active to interact with PVP. Therefore, it was the {111} planes that primarily adsorbed PVP when it was introduced. The adsorption stabilized the {111} plane and thus hindered the growth rate perpendicular to it. It resulted in the exposure of the {111} surfaces and produced truncated cubes. With the relative concentration of the modifier increasing, the surface energy of the {111} was further lowered. Thus, the gradual shrinkage of the {100} planes and the continuous enlargement of the {111} planes occurred. The proposed mechanism for the shape control of Cu_2O crystals achieved by preferential adsorption of PVP during the crystal growth process is summarized in Scheme 1.

The control experiments upon changing the molecular weight of PVP also agrees with the adsorption kinetics. For a polymer, the length of the molecular chain is proportional to its molecular weight. When the molecular weight of PVP was increased, the absorption dots would decrease owing to the space restriction, which would reduce its stabilization effect on the {111} planes. Therefore, PVP, with a larger molecular weight facilitated the increased ratio of $r\{100\}/r\{111\}$. As shown in Fig. 4, when the molecular weight of PVP was changed from M_w 30 000 to M_w 58 000, the morphology of the product switched from octahedrons (Fig. 4a) to cubooctahedrons (Fig. 4b), corresponding to the enlargement of {100} and the shrinkage of {111}. As shown in Fig. 4c, when the molecular weight of PVP increased to 630 000, the cubooctahedrons also dominated the products but with larger {100} areas than those in Fig. 4b. The molecular weight experiments provided further evidence for the selected adsorption of PVP on the {111} planes of Cu_2O crystals.

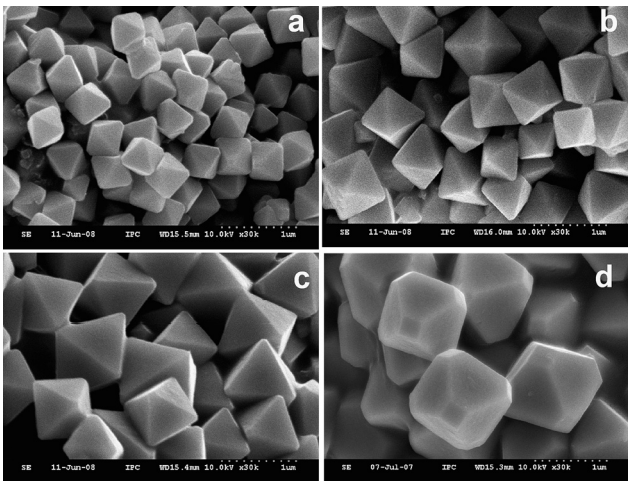

Fig. 5 FESEM images of the Cu_2O octahedrons produced under different temperatures for 3 h with $R = 30$. (a) 25, (b) 40, (c) 55, (d) 75 °C.

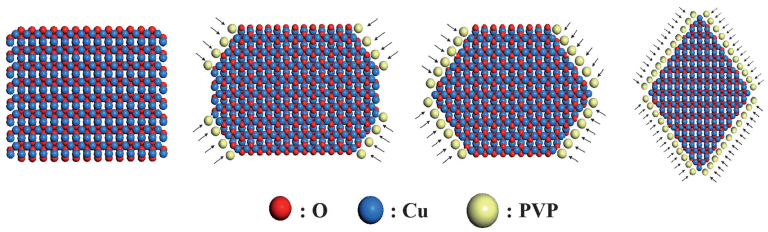

Scheme 1 Possible scheme of PVP modification during the shape evolution of Cu_2O crystals.

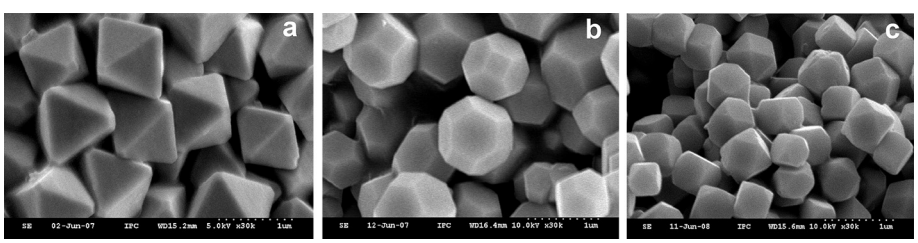

Fig. 4 FESEM images of the Cu_2O polyhedrons synthesized at 55 °C for 3 h with $R = 30$ using different molecular weights of PVP as capping agent. (a) 30 000, (b) 58 000, and (c) 630 000.

In addition to the tunable crystallographic surfaces, size control was also achieved by adjustment of the reaction temperature. Fig. 5a–c presents the cases for octahedrons obtained at different temperatures. As depicted in Fig. 5a–c, the sizes of the octahedrons increased from 400 to 850 nm when the temperature was increased from 25 to 55 °C. The accelerated growth rate under higher temperatures is believed to responsible for the size increase. However, when the temperature was further increased higher than 55 °C, no obvious size enlargement was observed although geometry variations were observed. As shown in Fig. 5d, the products developed into {100}-truncated octahedrons at 75 °C. It is well known that molecular thermal motion is intensified with elevated temperature. The higher temperature would move the adsorption–desorption balance towards the desorption direction. Thus, the surface energy of {111} is heightened to some extent and the growth ratio along [111] *versus* [100] increased, which produced the truncated octahedrons.

To demonstrate the potential application of the as-prepared Cu_2O nanocrystals and the relation to the exposed crystallographic facets, we investigated the adsorption ability of the different shaped nanocrystals (such as cube, cubooctahedron, and octahedron) with methyl orange (MeO) as the pollutant. The experiments were carried out with Cu_2O dispersed in the solution of MeO in the dark for various durations with constant stirring.

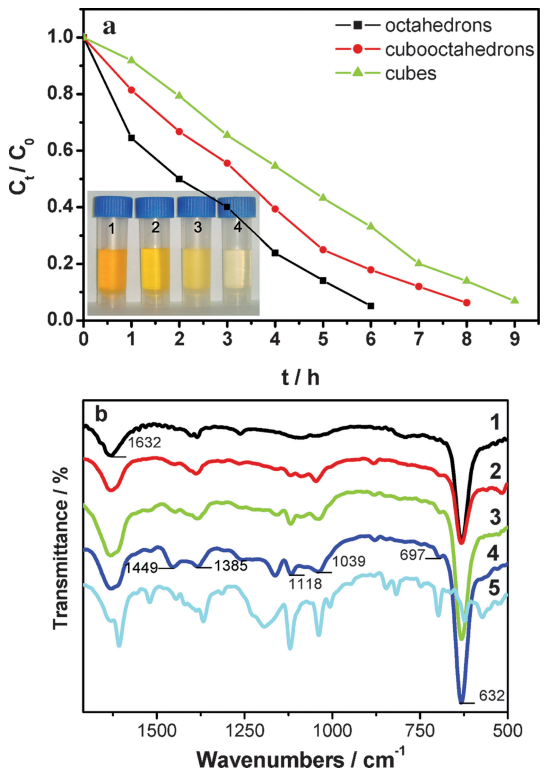

Fig. 6 (a) Absorption spectra of the aqueous solution of methyl orange (15 mg L^{-1}, 100 mL) in the presence of Cu_2O (0.05 g) with different geometries at different intervals. The inset shows the photographs of MeO solutions after adsorption by Cu_2O octahedrons at 0, 2, 4, and 6 h, respectively. (b) The FTIR spectra of (1) Cu_2O nanocubes before MeO adsorption, (2–4) the residual after the MeO adsorption by Cu_2O nanocubes, cubooctahedrons, octahedrons, respectively, and (5) the pure MeO.

After centrifugation, the UV-Vis absorption of the supernatant was measured and the characteristic absorption of MeO at about 465 nm was selected to monitor the adsorption process. As illustrated in Fig. 6a, the concentration of the MeO progressively decreased and lowered to about 6% after about 6 h, 8 h and 9 h for Cu_2O octahedrons, cubooctahedrons and cubes, respectively. The inset shows the corresponding photograph of the MeO solution in the presence of Cu_2O octahedrons at different intervals, which provided vivid pictures for the progressive decolorization process from orange, light orange to colorless. Since the mixing was carried out in the dark, the decolorization should result from the adsorption of Cu_2O particles, which is further corroborated by the Fourier transform infrared (FTIR) analysis (Fig. 6b). The FTIR spectrum of the Cu_2O particles before adsorption exhibits two strong vibration bands as shown in curve 1 in Fig. 6b. The band at 632 cm^{-1} corresponds to the Cu–O bond [27] (optically active lattice vibration in the oxide), and the peak at 1632 cm^{-1} is attributed to the –OH bending vibration, which originates from the surface-adsorbed H_2O. In comparison with the FTIR spectrum of the pure Cu_2O nanocubes, some new peaks appear in those of Cu_2O after adsorption (curves 2–4 in Fig. 6b). Combined with the FTIR of pure MeO (curve 5 in Fig. 6b), the new peaks can be assigned to the characteristic vibration from MeO. The peaks at 1449 cm^{-1} and 1385 cm^{-1} are the signals from the methyl group. The peaks at 697 cm^{-1}, 1039 cm^{-1} and 1118 cm^{-1} come from the vibration of the sulfonic group.[28] Thus, the FTIR characterization provided solid evidence for the MeO adsorption by Cu_2O nanocrystalline polyhedra.

Obviously, the adsorption ability of MeO to the different shaped Cu_2O nanocrystals follows the sequence of octahedrons > cubooctahedrons > cubes. Considering their crystallography, it can be concluded that the adsorption ability to MeO has a close relationship with the exposed {111} surface area. The larger the {111} surface area is, the higher the adsorption rate of MeO is. As described above, the {111} surfaces possess active 'Cu' atoms, which tend to interact with negatively charged MeO (*i.e.* $-SO_3^-$). Thus, the geometries with larger exposed {111} surface areas would adsorb more MeO, especially at the initial stage. It is coincident with the preferential adsorption of PVP towards {111} planes.

Conclusion

In summary, we demonstrated a simple approach to achieve the crystallographic surface construction of Cu_2O, where no preformed crystal was added as a sacrificial template. The preferential adsorption of PVP on the {111} facets of cubic Cu_2O made it possible to delicately control the volume fraction ratio of {100} to {111} and thus, their final geometries. The detailed modifying mechanism was elucidated based on the intrinsic structural nature of Cu_2O and PVP. The synthesis possesses advantages such as mass production, easy operation and high reproducibility, and may represent a new way to systematically direct the morphology transformation for other semiconductor materials. The adsorption investigations with MeO as the pollutant exhibited good surface-dependent activities. The as-prepared products are expected have potential applications in catalysis,

sensors and optoelectronics, where their properties depend on the different crystallographic planes of the crystals.

Acknowledgements

Authors acknowledge the support from the NSFC (20725208 & 20803002), NCET (06-0175), State Key Project of Fundamental Research for Nanoscience and Nanotechnology (2006CB932301 & 2007CB935400), Funding Project for Academic Human Resources Development in Institutions of Higher Learning under the Jurisdiction of Beijing Municipality and the Research Fund for the Doctoral Program of Higher Education of China (No. 20070006016).

References

1 A. R. Tao, S. Habas and P. D. Yang, *Small*, 2008, **4**, 310.
2 N. Tian, Z. Y. Zhou, S. G. Sun, Y. Ding and Z. L. Wang, *Science*, 2007, **316**, 732.
3 H. L. Xu, W. Z. Wang and W. Zhu, *J. Phys. Chem. B*, 2006, **110**, 13829.
4 J. G. Chen, B. J. Wiley and Y. N. Xia, *Langmuir*, 2007, **23**, 4120.
5 D. Seo, C. I. Yoo, J. C. Park, S. M. Park, S. Ryu and H. Song, *Angew. Chem., Int. Ed.*, 2008, **47**, 763.
6 K. H. Schulz and D. F. Cox, *J. Catal.*, 1993, **143**, 464.
7 P. E. de Jongh, D. Vanmaekelbergh and J. J. Kelly, *Chem. Commun.*, 1999, 1069.
8 J. Zen, Y. S. Song, H. H. Chung, C. T. Hsu and A. S. Kumar, *Anal. Chem.*, 2002, **74**, 6126.
9 T. Kuykendall, P. J. Pauzauskie, Y. F. Zhang, J. Goldberger, D. Sirbuly, J. Denlinger and P. D. Yang, *Nat. Mater.*, 2004, **3**, 524.
10 A. F. Wells, *Structural Inorganic Chemistry*, Clarendon, Oxford, 5th edn, 1984.
11 J. Xu, S. Li, J. Weng, X. F. Wang, Z. M. Zhou, K. Yang, M. Liu, X. Chen, Q. Cui, M. Y. Cao and Q. Q. Zhang, *Adv. Funct. Mater.*, 2008, **18**, 277.
12 L. F. Gou and C. J. Murphy, *Nano Lett.*, 2003, **3**, 231.
13 H. L. Xu and W. Z. Wang, *Angew. Chem., Int. Ed.*, 2007, **46**, 1489.
14 J. T. Zhang, J. F. Liu, Q. Peng, X. Wang and Y. D. Li, *Chem. Mater.*, 2006, **18**, 867.
15 C. C. Li, K. L. Shuford, M. H. Chen, E. J. Lee and S. O. Cho, *ACS Nano*, 2008, **2**, 1760.
16 B. J. Wiley, Y. Chen, J. M. McLellan, Y. J. Xiong, Z. Y. Li, D. Ginger and Y. N. Xia, *Nano Lett.*, 2007, **7**, 1032.
17 S. H. Im, Y. T. Lee, B. Wiley and Y. N. Xia, *Angew. Chem., Int. Ed.*, 2005, **44**, 2154.
18 T. R. Zhang, W. J. Dong, M. Keeter-Brewer, S. Konar, R. N. Njabon and Z. R. Tian, *J. Am. Chem. Soc.*, 2006, **128**, 10960.
19 H. L. Cao, X. F. Qian, J. T. Zai, J. Yin and Z. K. Zhu, *Chem. Commun.*, 2006, 4548.
20 H. Zhang, X. Ren and Z. L. Cui, *J. Cryst. Growth*, 2007, **304**, 206.
21 Z. T. Zhang, B. Zhao and L. M. Hu, *J. Solid State Chem.*, 1996, **121**, 105.
22 M. J. Siegfried and K. S. Choi, *Adv. Mater.*, 2004, **16**, 1743.
23 M. J. Siegfried and K. S. Choi, *J. Am. Chem. Soc.*, 2006, **128**, 10356.
24 C. J. Murphy, *Science*, 2002, **298**, 2139.
25 Z. L. Wang and X. D. Feng, *J. Phys. Chem. B*, 2003, **107**, 13563.
26 N. Wang, X. Cao, L. Guo, S. H. Yang and Z. Y. Wu, *ACS Nano*, 2008, **2**, 184.
27 C. O. Zorica, A. Alojz, D. Goran and Z. Majda, *Cryst. Growth Des.*, 2007, **7**, 453.
28 F. Chen, Y. Xie and J. J. He, *J. Photochem. Photobiol., A*, 2001, **138**, 139.